#### **PAPER • OPEN ACCESS**

# Using tensile and compressive stress superposition during incremental forming to manipulate martensitic transformation in SS304

To cite this article: E M Mamros et al 2024 IOP Conf. Ser.: Mater. Sci. Eng. 1307 012006

View the article online for updates and enhancements.

## You may also like

- Process variables optimization for multiple responses in SPIF of titanium using Taguchi-GRA
- Bibek Jyoti Dutta and Pankaj Chandna
- Noninvasive quantification of nonhuman primate dynamic <sup>18</sup>F-FDG PET imaging Xueqi Chen, Sulei Zhang, Jianhua Zhang et al
- Shape measurement system for single point incremental forming (SPIF) manufacts by using trinocular vision and random pattern
- Francesco Setti, Ruggero Bini, Massimo Lunardelli et al.



## Using tensile and compressive stress superposition during incremental forming to manipulate martensitic transformation in SS304

## E M Mamros<sup>1\*</sup>, F Maaβ<sup>2</sup>, A E Tekkaya<sup>2</sup>, B L Kinsey<sup>3</sup>, and J Ha<sup>3</sup>

elizabeth.mamros@bucknell.edu

Abstract. Single point incremental forming (SPIF) is a flexible manufacturing process that has applications in industries ranging from biomedical to automotive. In addition to rapid prototyping, which requires easy adaptations in geometry or material for design changes, control of the final part properties is desired. One strategy that can be implemented is stress superposition, which is the application of additional stresses during an existing manufacturing process. Tensile and compressive stresses applied during SPIF showed significant effects on the resulting microstructure in stainless steel 304 truncated square pyramids. Specifically, the amount of martensitic transformation was increased through stress superposed incremental forming. Finite element analyses with advanced material modeling supported that the stress triaxiality had a larger effect than the Lode angle parameter on the phase transformation that occurred during deformation. By controlling the amount of tensile and compressive stresses superposed during incremental forming, the microstructure of the final component can be manipulated based on the intended application and desired final part properties.

## 1. Introduction

For creating the highly customizable components required in, e.g., the biomedical and automotive, industries, flexible manufacturing processes are desired. Incremental forming is one example of a rapid prototyping process that can achieve this objective without the use of custom tooling. The conventional single point incremental forming (SPIF) process simply requires a milling machine, hemispherical tool, and support frame for the blank to implement in an industrial environment. During SPIF, a user-defined toolpath guides the tool in a layer-by-layer manner to impose local deformation until the desired geometry is achieved. Incremental forming is a combination of bending, tension, and shear deformation mechanisms [1].

Stress superposition is a used in manufacturing to increase material formability, decrease the required forming loads, and enable customization of components [2]. Alternatively, the stress superposition strategy can be adopted to manufacture functionally graded parts using stress state sensitive microstructure changes, e.g., martensite transformation [3], in metals. These heterogeneous parts are

<sup>&</sup>lt;sup>1</sup> Department of Mechanical Engineering, Bucknell University, Lewisburg, PA, USA

<sup>&</sup>lt;sup>2</sup> Institute of Forming Technology and Lightweight Components, TU Dortmund University, Dortmund, Germany

<sup>&</sup>lt;sup>3</sup> Department of Mechanical Engineering, University of New Hampshire, Durham, NH, USA

Content from this work may be used under the terms of the Creative Commons Attribution 4.0 licence. Any further distribution of this work must maintain attribution to the author(s) and the title of the work, journal citation and DOI.

doi:10.1088/1757-899X/1307/1/012006

advantageous for applications requiring highly customized parts. Stress-superposed incremental forming (SSIF) variants, such as tensile (TSSIF) and compressive (CSSIF), have been proposed to control the material and final part properties. For instance, a polyurethane (PU) die was introduced when forming aluminum alloy 5083 to superpose compressive stresses into the SPIF process, CSSIF, which affected the residual stress development [4]. For TSSIF, investigations have used a custom tensile frame to examine the effect on residual stresses [5]. Note that the phase transformation behavior of the material can be directly influenced by manipulating the stress state or other parameters, including the temperature in the forming zone, strain rate, equivalent plastic strain level, and material orientation [6], during manufacturing processes.

In this paper, SPIF and three SSIF variants, TSSIF, CSSIF, and tensile compressive stress-superposed incremental forming (TCSSIF), were investigated experimentally and numerically for a truncated square pyramid. The primary objective was to determine the effect of the different stress states during deformation on the properties, e.g., the phase transformation, of the final product. An isotropic, combined strain hardening law for constituent phases was identified to model SS304 and coupled with the Beese and Mohr 2011 martensitic transformation kinetics model [7]. This material model was implemented into Abaqus 2019 [8] for each process using a two-step approach [3]. The numerical results were validated by experimental results for all four IF processes. A Feritscope was used to measure the  $\alpha$ '-martensite volume fraction on the formed parts. Collectively, these results support that stress superposition can be used in incremental forming to customize product properties and achieve functionally graded parts for specific applications, e.g., biomedical trauma fixation hardware.

#### 2. Material Characterization

SS304 sheets with an initial thickness of 0.8 mm were characterized by uniaxial tension, bulge, in-plane torsion, and disk compression experiments. The resulting  $\alpha$ '-martensite volume fractions were measured using an FMP30 Feritscope (Fischer Technology Inc.) and validated by electron backscatter diffraction. Further details regarding the material characterization experiments and Feritscope validation can be found in [3]. The Young's Modulus is approximately 170 GPa calculated from the stress-strain curve of uniaxial tension in the rolling direction (RD), and the Poisson's ratio is 0.33 based on the textbook value.

## 3. Constitutive Modeling

The SS304 material behavior, including phase transformation, was assumed to be isotropic for simplicity in modeling. An overview of the constitutive modeling is described below and summarized in Table 1. Additional details, including experimental data, can be found in [3].

Swift strain hardening models were used to describe the behavior of the constituent phases, i.e.,  $\gamma$ -austenite and  $\alpha$ '-martensite, individually. Then, these true stress-strain curves were combined in a weighted equivalent stress equation, which is a function of the phase volume fraction, i.e., the  $\alpha$ '-martensite volume fraction denoted by  $f_{\alpha\prime}$ .

The martensitic transformation kinetics was described using the isotropic Beese and Mohr 2011 model [7]. Based on experiments, Beese and Mohr expanded the definition of the stress state to include the Lode angle parameter,  $\bar{\theta}$ , in addition to stress triaxiality,  $\eta$ . This model assumes isothermal conditions, and the maximum achievable volume fraction,  $c_{\text{max}}$ , is dictated by the temperature value. The transformation kinetics order from greatest to least with respect to equivalent plastic strain for SS304 is: shear, equibiaxial tension, uniaxial tension, and uniaxial compression [3]. Note that this order is dependent on the specific SS material and component form investigated [2].

PU 90° Shore A was chosen for the die material. To characterize this material, cyclic compression experiments were conducted according to ISO 7743 [9]. In each experiment, a cylindrical specimen with an initial height of 30 mm and initial diameter of 20.5 mm was subjected to three compressive cycles. Three repetitions were conducted to ensure consistency of the results. For modeling the PU die, a hyperelastic material model was used, which derives the stress-strain relation from the deformation energy density. According to the Mooney-Rivlin model [10], the dependence of the strain energy density (MJ/m³) on the deformation is expressed by a polynomial equation with the strain invariants of the

Cauchy-Green strain tensor,  $I_1$  and  $I_2$ , [11]. However, for N=1, the Mooney-Rivlin model reduces to the two-parameter form with  $C_{10}$  and  $C_{01}$ . The parameters required for the simulation were calculated using Abaqus from the experimental data. Their values were  $C_{10}=1.714$  MPa and  $C_{01}=-0.186$  MPa.

<b>Table 1.</b> SS304 isotropic strain hardening and ma	ening and martensitic transformation kinetics modeling summary.		
Charles bondaning and del	Mantanaitia tuanafannatian madal		

	Strain hardening model			Martensitic transformation model							
$\bar{\sigma} = f_{\alpha\prime} \cdot \sigma_{\alpha\prime} + (1 - f_{\alpha\prime}) \cdot \sigma_{\gamma}$					$\dot{c} = (c_{\max} - c)nD(D\bar{\varepsilon})^{n-1}\dot{\bar{\varepsilon}}$						
Swift model					Stress state dependency						
	$\sigma = K(\varepsilon_0 + \bar{\varepsilon})^b$					$D = D(\eta, \bar{\theta}) = (D_0 + a_\theta \bar{\theta} + a_\eta \eta)_+$					
		K (MPa)	$\varepsilon_0$	b	l			D	_	a	
	$\sigma_{lpha'}$	1547	0.002	0.11	Ц	c <sub>max</sub>	n	$D_0$	$a_{\theta}$	$a_{\eta}$	
	$\sigma_{\gamma}$	1313	0.050	0.36		0.49	2.13	2.05	0.10	0.46	

## 4. Incremental Forming Experiments

The conventional incremental forming process, SPIF, and three variants with stress superposition, TSSIF, CSSIF, and TCSSIF were investigated. For consistency purposes, the same toolpath and general experimental setup were used for all four forming processes. The specimens were laser cut from SS304 sheets of 0.8 mm thickness into the shape shown in Figure 1. The bottom surface of each specimen, i.e., non-toolside, was electrochemically etched with a dot pattern to allow for strain and geometry measurements via a photogrammetry camera after forming. An 85 mm base truncated square pyramid with a 45° wall angle was the target geometry and is shown in Figure 1.

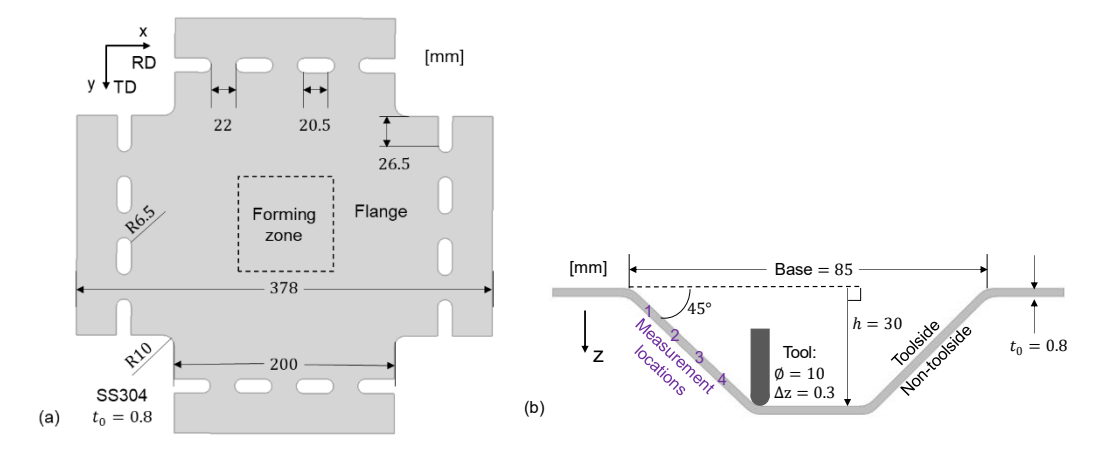


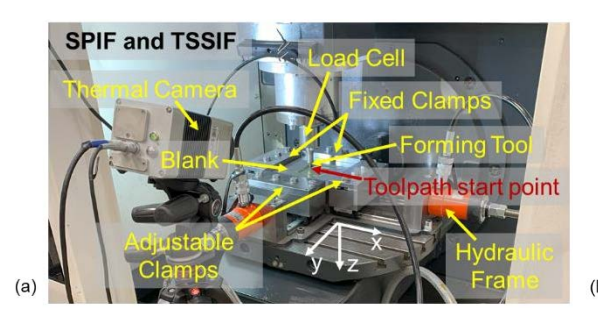
Figure 1. Incremental forming (a) blank, (b) target, and forming tool geometries.

The incremental forming experiments were conducted using a 5-axis DMU50 milling machine (DMG Mori). The machine's computer numerical controller was programmed to follow a user-defined, bidirectional toolpath, and the start point for each layer was located at the corner farthest from the two cylinders of the frame as indicated in Figure 2. For all process variants, a fixed (spindle rotation = 0 rpm), hemispherical tool with a 10 mm diameter tip was used with a step down of 0.3 mm and constant feed rate of 1500 mm/min, which resulted in a total forming time of ~811 s for the 30 mm depth. The base of the square truncated pyramid was formed first, i.e., an outside-in strategy was employed. A thin layer of deep-drawing oil (Castrol) was applied to the surface of the sheet prior to each experiment. A custom hydraulic frame was installed to act as a blankholder (Figure 2a), and during SPIF, a minimal pressure (< 5 bar) was applied to the hydraulic cylinders to fix the sheet specimens in-plane at the initial gripped position. The sheet blank was aligned such that the RD coincided with the x-axis of the setup.

The hydraulic frame shown in Figure 2a was used to superpose equibiaxial tensile stress to the SPIF

process for two SSIF variants: TSSIF and TCSSIF. For both cases, the frame was set to its maximum pressure, i.e.,  $\sim$ 200 bar for each cylinder, to apply in-plane equibiaxial tension to the sheet metal blank. Digital Image Correlation (DIC) measured that the von Mises strain (equivalent strain by von Mises yield function) achieved across the forming area is  $\sim$ 0.01.

To superpose compressive stress to SPIF, a PU die (190 mm x 190 mm x 50 mm) was used with the experimental setup described previously to form two SSIF variants: CSSIF and TCSSIF. A riser is placed in the center of the forming section in the tensile frame and holds the die securely (Figure 2b). The negative die cavity was milled into the surface of the die to the target geometry dimensions. Thus, a compressive phenomenon, so-called squeeze factor in DSIF, proportional to the sheet thickness, was applied at the tool contact point with the sheet during forming. A thin layer of lubricant was applied to the surface of the die cavity between experiments. Note that the die and die riser were removed from the experimental setup for SPIF and TSSIF experiments.



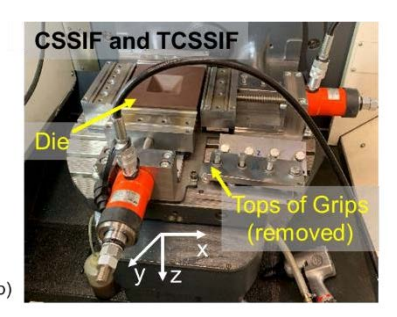


Figure 2. Experimental setup: (a) SPIF and TSSIF; and with die added for (b) CSSIF and TCSSIF.

### 5. Numerical modeling

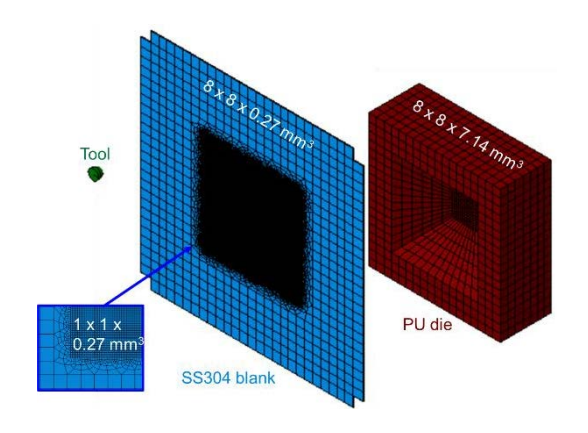
An overview of the numerical model created for the SPIF process is described below and detailed further in [5]. The SPIF finite element (FE) model is used and modified as necessary for the SSIF process variants. For TSSIF and TCSSIF, an additional simulation step was required to model the tensile stress superposition. For CSSIF and TCSSIF, another component was required in the model assembly to represent the PU die. For all processes, a two-step approach was used: 1) a full incremental forming process simulation using Abaqus/Explicit 2019 with only isotropic elastic-plastic models, i.e., Hooke's law combined with von Mises yield function and Swift strain hardening, not considering phase transformation, to determine the strain in a given element at a specified location; 2) one element simulations using Abaqus/Implicit 2019 with isotropic elastic-plastic models with martensite transformation kinetics, which were implemented into a user material subroutine (UMAT), to predict the transformation at select locations (Section 5.1). Note that this was not a thermal-mechanical analysis.

The SPIF process was modeled using linear brick elements with reduced integration, C3D8R, for the sheet with three elements through the sheet thickness direction. Note that a simplified sheet geometry was used in the model that excluded part of the gripped region. A subsection of the forming area that is larger than the target geometry contained a refined mesh for increased accuracy. A transition zone is partitioned around this subsection, and the remaining flange area was coarsely meshed to increase computational efficiency(Figure 3). Mass scaling of  $10^3$  was used. Mesh and mass scaling convergence studies were completed. The tool was modeled as a rigid body. The toolpath used for experiments was converted from G-code to amplitudes and step times based on the length of each toolpath layer. This converted toolpath was implemented as displacement boundary conditions without time scaling. Due to the presence of lubrication on one or both sides of the sheet, depending on the chosen IF process, friction between the tool and the sheet on the toolside and between the sheet and the die on the non-toolside were ignored, i.e., the friction coefficient,  $\mu = 0$ .

To superpose tensile stress in the numerical model, a step for pre-stress was added to the TSSIF and TCSSIF simulations. During this step, the tool and the clamped, i.e., -x and -y, sides of the blank were fixed. Displacement boundary conditions were applied to the adjustable, i.e., +x and +y, sides of the

blank. The displacement value, i.e., 1.975 mm, was chosen to create approximately 1% von Mises strain in the forming area to replicate the DIC experimental results of the loaded blank in the tensile frame.

To superpose the compressive stress in the numerical model, the PU die was included in the assembly as a deformable body. PU 90° Shore A was modeled based on the results in Section 3. The die contained 2988 elements (type C3D8R) with seven elements through the thickness and is shown in Figure 3. The interaction between the die and the sheet was modeled as kinematic contact. An additional boundary condition was applied to impose the displacement restrictions on the riser used in experiments.



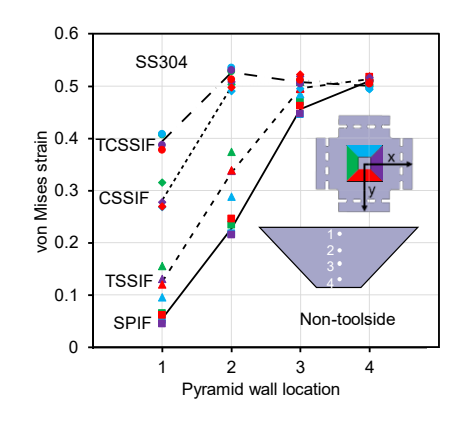


**Figure 3.** FE model assembly for CSSIF and TCSSIF: exploded isometric view.

**Figure 4.** von Mises strain at locations 1-4 on the non-toolside (Exp.). Averages are shown as lines.

#### 5.1. One element simulation for martensitic phase transformation

One element, implicit simulations were used to predict the phase transformation along the pyramid walls at the same locations as the Feritscope measurements. The nodal displacements from 12 elements for each incremental forming variant, i.e., four elements from the toolside, midplane, and non-toolside, from the full model simulations were exported and prescribed as the boundary conditions for the one element simulations. The isotropic strain hardening and martensitic transformation kinetics models were combined in the UMAT to describe the deformation induced phase transformation in the sheet specimens during stress-superposed incremental forming. This two-step method is both computationally efficient and provides information not readily available experimentally, e.g., the volume fractions at the midplane along the thickness direction, which cannot be measured directly using the Feritscope.

#### 6. Results and discussion

The von Mises final strain states from experiments at locations 1-4 on the non-toolside are shown in Figure 4. The largest difference in strain between the processes was observed at location 1. TCSSIF had the highest strain, followed by CSSIF, then TSSIF, and, lastly, SPIF with the lowest strain. At location 2, the same order applies although the difference between the processes decreased. At location 3, the strains for the IF processes start to converge, and at location 4, they are nearly equal. This trend is also in agreement with the assumption that the effectiveness of the stress superposition varies throughout the forming process. Based on the trends in Figure 6, the stress superposition had the greatest effect when the strain increased significantly between locations. Explicitly, the compressive stress superposition appears to be the most effective from locations 1 to 2 (see the largest von Mises strain increase for the CSSIF case), while the tensile stress superposition effect was sustained from locations 1 to 3. As a result, the contributions of each type of stress superposition caused the von Mises strain results for the TCSSIF case. Further analysis into the hierarchy of the forming mechanisms for each process at each location is warranted to improve the understanding of these observations.

From the chosen martensitic transformation kinetics model, the stress state can be described by two quantities: the stress triaxiality and Lode angle parameter. Figure 5 shows the evolution of the stress state throughout the forming process for each IF process with respect to the equivalent plastic strain.

These results were extracted from the full model simulations and filtered based on the equivalent plastic strain increment, which represents the effective plastic deformation for the martensite transformation. Note that a material point (or element in FE simulation) deforms a very small strain increment, and the associated stress state change does not significantly impact the martensite transformation, when the tool is located far away from the element of interest, e.g., on other pyramid walls. Thus, only steps which contained an equivalent plastic strain increase  $\Delta \bar{\epsilon} > 0.001$  are plotted.

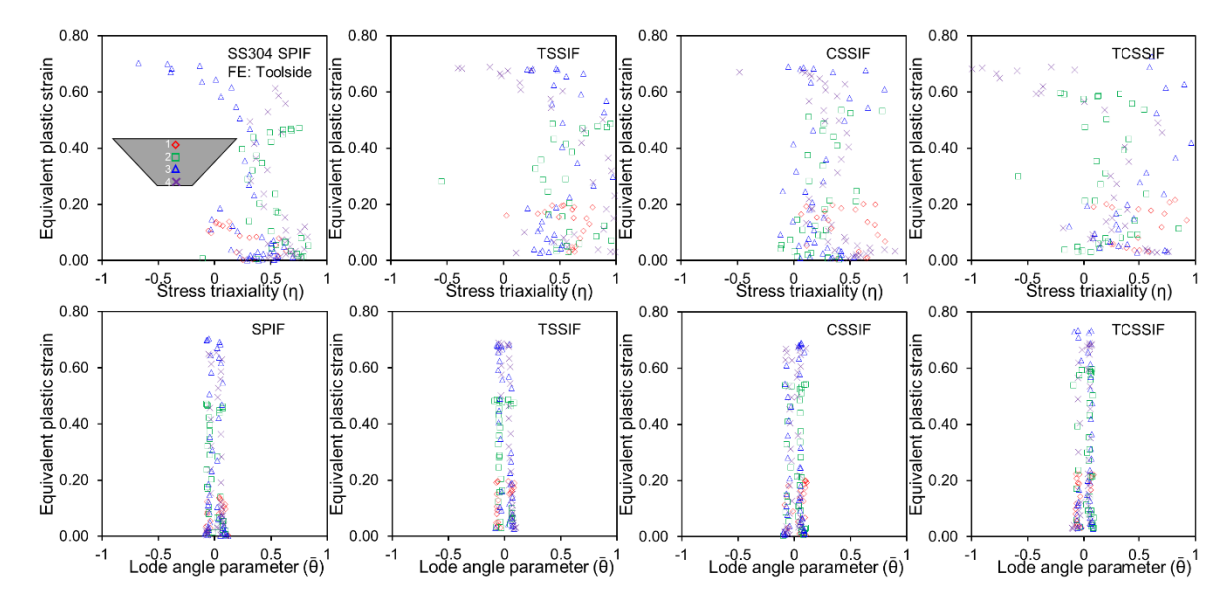


Figure 5. Stress state evolutions from full FE models of IF processes on toolside at locations 1-4.

For all four processes, the Lode angle parameter showed less variation than the stress triaxiality during forming. At low levels of equivalent plastic strain, i.e., < 0.1, the spread of Lode angle parameter values was larger than at higher levels of equivalent plastic strain, where it fluctuated between -0.2 and 0.2. A Lode angle parameter value close to 0 indicates generalized shear, which is expected due to the presence and contact of the tool on this side of the sheet. However, the stress triaxiality showed stronger evolution and different trends for each of the forming processes with respect to equivalent plastic strain. Near location 1, the stress triaxiality was positive for all four processes with values indicative of generalized shear ( $\eta = 0$ ), uniaxial tension ( $\eta = 0.33$ ), plane strain tension ( $\eta = 0.58$ ), and equibiaxial tension ( $\eta = 0.67$ ). For SPIF, near location 3, the stress triaxiality trended toward negative values, which indicate compression ( $\eta = -0.33$ ) and biaxial compression ( $\eta = -0.67$ ). For TSSIF, the stress triaxiality remained positive for the majority of the process but started to trend toward zero, i.e., shear, at locations 3 and 4. For CSSIF, the stress triaxiality initially trends toward zero values for all four locations, but near locations 2 and 3, it curves toward positive values. For TCSSIF, all four locations started with positive stress triaxialities, and then locations 2 and 4 trended towards negative values.

These differing trends can be attributed to the process variations but also provide information related to the effectiveness of the stress superposition throughout the process. For example, in TSSIF, the stress triaxiality remains positive throughout the majority of the process due to the tensile stress superposition rather than trending towards negative values later like SPIF. This result of stress triaxiality closer to uniaxial tension rather than uniaxial compression resulting in increased phase transformation for TSSIF compared to SPIF is consistent with the martensitic transformation kinetics trend with respect to stress state. For the CSSIF and TCSSIF, the effectiveness of the die seemingly increased at locations 3 and 4 as a result of greater contact with the tool at larger forming depths. The variation in the stress state, particularly stress triaxiality, for each process also had significant effects on the phase transformation.

To analyze the martensitic transformation, first, the ferrite number was measured on the toolside at four locations along each pyramid wall (as shown in Figure 1b) by an FMP30 Feritscope, and the  $\alpha$ '-

martensite volume fraction,  $f_{\alpha\prime}$ , was calculated using the preprogrammed conversion factor. The same methodology was repeated for the non-toolside, and the results are shown in Figure 6. The measurements on the non-toolside were consistently lower than the toolside by  $\sim 0.1~\alpha$ '-martensite but show the same trends. This observation is consistent with the deformation mechanisms of SPIF, which include increased deformation on the toolside.

Comparing Figures 4 and 6, the four processes followed the same trend with respect to one another for all four locations on the non-toolside. TCSSIF had the highest von Mises strain and phase transformation, followed by CSSIF, then TSSIF, and lastly SPIF. Between locations 1 and 2, the von Mises strain and  $\alpha$ '-martensite volume fraction increased for all processes except for TCSSIF, which experienced a slight decrease in phase transformation. This is likely the result of the decreasing effectiveness of the tension stress superposition as the forming process progressed, which is reflected in the stress triaxiality evolution towards compression. From location 3 to location 4, the von Mises strain and  $\alpha$ '-martensite volume fractions converged for all processes. Increased von Mises strain leads to increased phase transformation; contrastingly, increased temperature inhibits phase transformation. Further investigations are warranted to determine the weighted contributions of these factors.

To explain the variation in the Feritscope measurements for the four pyramid walls, two possible explanations are the material anisotropy and the frame in the experimental setup. Since two sides of the frame are fixed and the loading is only applied to the remaining two sides, the loading is not perfectly equibiaxial tension with variations in the biaxial stress state applied on the four sides. Although not considered in this work, anisotropy with respect to martensitic transformation is possible [7].

The  $\alpha$ '-martensite volume fractions predicted by the one element simulations and measured from experiments are shown in Figure 6. The error bars on the experimental results represent the maximum error, which includes the variation between the four walls of the truncated square pyramids, the repeated Feritscope measurements at each location, and the multiple samples for each process. In addition to the toolside and non-toolside predictions, the FE model also provided data related to the midplane of the pyramid walls, which cannot be measured directly using the Feritscope.

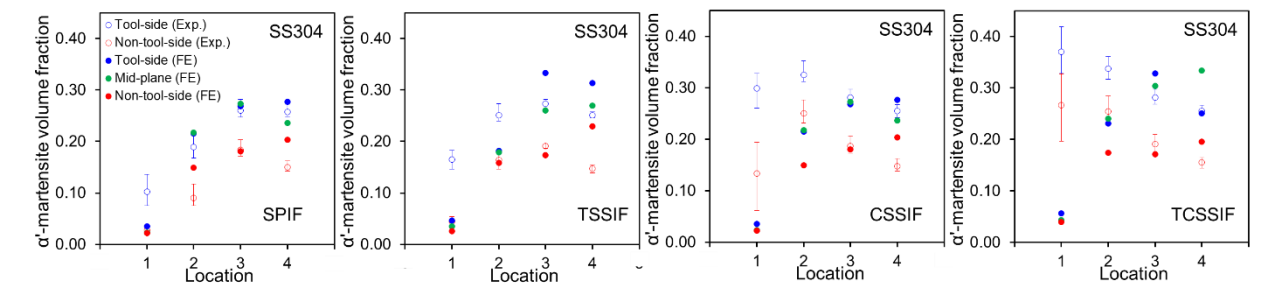


**Figure 6** Comparison of  $\alpha'$ -martensite volume fraction measurements from Feritscope (Exp.) with predictions from one element simulations (FE).

In general, the one element simulations provided fair predictions of the  $\alpha$ '-martensite volume fractions compared to the experimental values without requiring significant additional computational expense. The implemented martensitic transformation kinetics model is able to capture increasing phase transformation trends with respect to the pyramid wall location well, e.g., SPIF locations 1-3. A limitation of the model is its inability to account for inhibited phase transformation at elevated temperatures, e.g., at location 4 for SPIF, TSSIF, and CSSIF. This two-step method could be optimized to be used with different martensitic transformation kinetics models to improve the predictions.

## 7. Conclusions and future work

The stress superposition of in-plane tensile and normal to the sheet compressive stresses during SPIF to manufacture a truncated square pyramid using SS304 was investigated for four IF variants: SPIF, TSSIF,

CSSIF, and TCSSIF. Final strain state, stress state evolution, and phase transformation results were analyzed and compared between process variants and experimental and numerical analyses.

A two-step FE method was utilized to further investigate the phase transformation mechanisms affecting the IF processes. SPIF, TSSIF, CSSIF, and TCSSIF revealed different trends with respect to the stress state evolution during the forming process. Particularly, the stress triaxiality showed greater variation than the Lode angle parameter, which remained close to generalized shear for locations 1 to 4. The different stress state evolutions between the processes affected the phase transformation at each location. However, the  $\alpha$ '-martensite volume fraction was ultimately impacted by several effects, including process temperature, equivalent plastic strain level, and stress state, which needed to be considered collectively. A Feritscope was used to measure the  $\alpha$ '-martensite volume fraction on the formed truncated square pyramids. At locations 1 and 2, TCSSIF had the greatest transformation, followed by CSSIF, then TSSIF, and SPIF had the least amount of transformation. At locations 3 and 4, the four processes converged to similar volume fractions of  $\alpha$ '-martensite. Future work is planned to establish a better understanding of the relationship between the martensitic transformation and residual stress development in SS304 during SSIF. However, the current results support that functionally graded, formed parts can be created from these manufacturing processes for implementation into several industries. For example, biomedical trauma fixation hardware requires patient-specific geometries and heterogeneous material properties, e.g., increased strength near the fixture locations of an implant.

#### References

- [1] Martins P A F, Bay N, Skjoedt M and Silva M B 2008 Theory of single point incremental forming *CIRP Annals* **57** 247–52
- [2] Tekkaya A E, Groche P, Kinsey B and Wang Z G 2023 Stress superposition in metal forming *CIRP Annals* **72** 621-644
- [3] Mamros E M, Maaß F, Hahn M, Tekkaya A E, Ha J and Kinsey B L 2023 Martensitic transformation of SS304 truncated square pyramid manufactured by single point incremental forming (submitted)
- [4] Maaß F, Hahn M and Tekkaya A E 2021 Adjusting residual stresses by flexible stress superposition in incremental sheet metal forming *Arch Appl Mech* **91** 3489–99
- [5] Maaß F, Hahn M and Tekkaya A E 2022 Setting Residual Stresses in Tensile Stress-superposed Incremental Sheet Forming *Proceedings of the 22nd International Conference on Material Forming* ESAFORM 2022
- [6] Feng Z, Mamros E M, Ha J, Kinsey B L and Knezevic M 2021 Modeling of plasticity-induced martensitic transformation to achieve hierarchical, heterogeneous, and tailored microstructures in stainless steels *CIRP Journal of Manufacturing Science and Technology* **33** 389–97
- [7] Beese A M and Mohr D 2011 Effect of stress triaxiality and Lode angle on the kinetics of strain-induced austenite-to-martensite transformation *Acta Materialia* **59** 2589–600
- [8] Hibbitt D, Karlsson B and Sorensen P 1978 Abaqus (Dassault Systèmes Simulia Corporation)
- [9] ISO 7743:2017 2017 Rubber, vulcanized or thermoplastic Determination of compression stress-strain properties (ISO)
- [10] Mooney M 1940 A Theory of Large Elastic Deformation Journal of Applied Physics 11 582–92

IOP Conf. Series: Materials Science and Engineering 1307 (2024) 012006

doi: 10.1088/1757 - 899X/1307/1/012006

[11] Stommel M, Stojek M and Korte W 2018 Mechanisches Werkstoffverhalten und -modellierung *FEM zur Berechnung von Kunststoff- und Elastomerbauteilen* (Carl Hanser Verlag GmbH & Co. KG) pp 5–144